Journal of Quantitative Spectroscopy & Radiative Transfer 357 (2026) 109879

Contents lists available at ScienceDirect

Journal of Quantitative Spectroscopy and Radiative Transfer

journal homepage: www.elsevier.com/locate/jqsrt

An improved study of cyanoacetylene and diacetylene including the strong $2\nu_5$ band of HC_3N and ν_4 band of HC_4H☆,☆☆

Luca Bizzocchi [a],*, Mattia Melosso [a],*, Filippo Tamassia [b],*, Martina Taddia [a,1], Francesca Tonolo [c], Silvia Alessandrini [a], Gabriele Panizzi [a], Michela Nonne [d], Marie-Aline Martin-Drumel [e], Olivier Pirali [e,f], Luca Dore [a], Iouli E. Gordon [g], Cristina Puzzarini [a]

[a] Dipartimento di Chimica "Giacomo Ciamician", Università di Bologna, Via P. Gobetti 85, 40129 Bologna, Italy
[b] Dipartimento di Chimica Industriale "Toso Montanari", Università di Bologna, Via P. Gobetti 85, 40129 Bologna, Italy
[c] Université de Rennes, CNRS, IPR (Institut de Physique de Rennes) – UMR 6251, 35000 Rennes, France
[d] Scuola Superiore Meridionale, Largo San Marcellino 10, 80138 Napoli, Italy
[e] Université Paris-Saclay, CNRS, Institut des Sciences Moléculaires d'Orsay, 91405 Orsay, France
[f] SOLEIL Synchrotron, AILES beamline, l'Orme des Merisiers, Saint-Aubin, 91190 Gif-sur-Yvette, France
[g] Harvard-Smithsonian Center for Astrophysics, Atomic and Molecular Physics Division, Cambridge, MA, USA

ARTICLE INFO

Keywords:
Cyanoacetylene
Diacetylene
Interstellar matter
Molecular spectroscopy
Spectroscopic database
Energy levels
Ro-vibrational spectra

ABSTRACT

This paper presents an extension of the previous spectroscopic investigations for the linear molecules HC_3N and HC_4H. For both species, new high-resolution data have been recorded and analyzed. As far as HC_3N is concerned, the investigation of the ro-vibrational features has been based on the Fourier transform far-infrared spectra from our previous studies and on the mid-infrared spectra targeting the prominent $2\nu_5$ overtone band recently recorded at the synchrotron facility SOLEIL with a resolution of 0.003 and 0.002 cm^{-1}. Moreover, several hundreds of pure rotational transitions belonging to excited vibrational states were recorded in Bologna. The resonance network wrapping around the $\upsilon_5 = 2$ level and involving the ($\upsilon_4 = 1, \upsilon_7 = 2$), ($\upsilon_6 = 2, \upsilon_7 = 2$), ($\upsilon_5 = 1, \upsilon_7 = 3$), and $\upsilon_7 = 6$ excited states has been thoroughly analyzed. A global ro-vibrational fit was then achieved for all the vibrational levels up to 1300 cm^{-1}, therefore improving our previous analysis. For diacetylene, the ν_4 stretching band around 3333 cm^{-1} was recorded by high-resolution FTIR spectroscopy at the synchrotron facility SOLEIL at a resolution of 0.005 cm^{-1}. The accidental resonance affecting this band has been successfully analyzed and the number of observed and assigned ro-vibrational transitions was considerably extended. The present investigation allowed the integration of the existing line lists in the HITRAN database for both molecules. In particular, no information about the ν_4 band of diacetylene was present in HITRAN before this study.

1. Introduction

A highly unsaturated carbon skeleton is found in many of the largest chemical structures discovered in the interstellar medium (ISM) [1,2]. Although a few cumulenic chains (C=C=C) have also been detected in the ISM, molecules based on the acetylene moiety (C≡C) are markedly more abundant and encompass a large variety of extra-terrestrial environments. Within these species, cyanopolyynes ($HC_{2n+1}N$) and polyacetylenes ($HC_{2n}H$) represent two of the most important chemical families and their parent members, cyanoacetylene (HC_3N) and diacetylene (HC_4H) — building blocks of longer and more complex structures, are among the most targeted species in astronomical studies. Due to its high dipole moment, HC_3N exhibits strong rotational emission features which are easy to detect by radio-telescopes, thus making its identification possible in almost all kind of astronomical objects (see Ref. [3] for a comprehensive but not exhaustive account). While HC_4H is likely to be quite abundant as well, its non-polar nature makes it much more elusive as its detection is only possible via infrared (IR) observations. Despite this, diacetylene is recognized as a key ingredient in some planetary atmospheres (such as Titan [4]) and it has been identified even outside our Galaxy, in the Large Magellanic Cloud [5].

☆ This article is part of a Special issue entitled: 'HITRAN 2024' published in Journal of Quantitative Spectroscopy and Radiative Transfer.
☆☆ Supplementary material available.

* Corresponding authors.
E-mail addresses: luca.bizzocchi@unibo.it (L. Bizzocchi), mattia.melosso2@unibo.it (M. Melosso), filippo.tamassia@unibo.it (F. Tamassia).
[1] Current affiliation: Consiglio Nazionale delle Ricerche, Istituto di Scienze dell'Atmosfera e del Clima (CNR-ISAC), Via P. Gobetti 101, 40129 Bologna, Italy.

https://doi.org/10.1016/j.jqsrt.2026.109879
Received 22 January 2026; Received in revised form 19 February 2026; Accepted 23 February 2026
Available online 5 March 2026

Because of their relevance, these two pivotal species have been targeted by intensive laboratory investigations, many of which were carried out by some of the authors. The most recent and comprehensive analysis of the ro-vibrational spectrum of HC_3N have been published by Tamassia et al. [6], where a full account of the relevant bibliography is reported (see also Ref. [3] for completeness). As far as HC_4H is concerned, we previously reported on the analysis of its IR [7] and millimeter-wave (mm-wave) spectra [8]. These papers, together with few earlier studies [9–12] and the more recent 3 μm-investigation of a jet-cooled sample by Zhao et al. [13], set the base of the current spectroscopic knowledge of HC_4H.

In spite of such considerable experimental efforts, the modeling of some prominent spectral features of both HC_3N and HC_4H is still not fully satisfactory. The $2\nu_5$ overtone of cyanoacetylene (H−C≡C bend), located at ca. 1313 cm^{-1}, is one of its strongest IR bands (see Figure 1 of Ref. [6]), but the $v_5 = 2$ state is involved in a complex network of anharmonic resonances, and the spectrum shows evidences of local perturbations [14]. Concerning HC_4H, the problematic band is the strong ν_4 (asymmetric C−H stretch) at ca. 3333 cm^{-1}, whose energy levels are in close degeneracy with a dark state manifold which produces conspicuous irregularities in the ro-vibrational line patterns of the fundamental and its hot-bands.

Here, we address these issues by presenting an improved spectroscopic characterization of the $2\nu_5$ band of HC_3N and the ν_4 fundamental of HC_4H, together with a detailed analysis of the associated resonance systems. In addition, for HC_3N the present analysis extends into the high-energy stretching region, where we have refined the modeling of the ν_1, ν_2, and ν_3 bands by (i) including additional hot-bands originating from the $v_7 = 2$ state, and (ii) explicitly treating the resonance interactions affecting the $v_1 = 1$ and $v_1 = v_7 = 1$ states [15]. This work aims at providing a more accurate description of the ro-vibrational energy manifolds of these two carbon-chain species, complementing and extending previous investigations.

2. Experiments

The present study is based on IR measurements performed on the AILES beamline of the SOLEIL synchrotron facility (France), and on additional mm- and submm-wave investigations conducted at the University of Bologna. The HC_3N spectra were recorded using the sample prepared for previous studies [3,6], whereas HC_4H was newly synthesized following the procedure described by Armitage et al. [16].

Briefly, 1,4-dichloro-2-butyne was dissolved in tetraethylene glycol dimethyl ether and heated to 65 °C. Then, a 16% aqueous solution of KOH was added slowly under vigorous stirring and reflux. The incondensable gas was led over anhydrous $CaCl_2$ by an Ar flow and then passed through a trap placed at −96 °C in a acetone slush bath. The collected sample consisted in almost pure diacetylene and was then utilized for the IR measurements without further manipulation. The sample degrades quickly by polymerization in solid phase and was thus kept a −96 °C for the few days needed for recording the spectra at SOLEIL.

The measurements at SOLEIL were performed using a Bruker IFS 125 FT interferometer [17] equipped with a 100 m optical path length White-type multi-pass absorption cell [18,19]. The mid-IR spectrum of HC_3N was initially recorded in the 600–4500 cm^{-1} interval, summing up some 800 scans at a pressure of 100 μbar. The resolution was set to 0.003 cm^{-1}. A Globar was employed as a source, with a KBr beamsplitter and a HgCdTe (MCT) detector [20]. An additional recording in the 600–1500 cm^{-1} wavenumber range was performed at the pressure of ∼ 2 μbar and at 0.002 cm^{-1} resolution. As far as HC_4H is concerned, its IR spectrum was recorded in the 1980–8700 cm^{-1} range. Three different sample pressures were employed: we co-added 140 scans at 0.5 μbar, 200 scans at 3 μbar, and 414 scans at 50 μbar. We used a near-infrared source with CaF_2 beamsplitter and MCT detector. The resolution was set to 0.005 cm^{-1}.

New mm- and submm-wave spectra of HC_3N have been recorded at the University of Bologna. The 61–500 GHz frequency interval has been covered almost continuously using a frequency-modulation mm-wave spectrometer, whose detailed description is given elsewhere [21,22]. Most of the spectra have been acquired using a W-band Signal Generator Extension module (WR10SGX-M, Virginia Diode Inc.) fed by a 10 dBm signal generated by a centimeter-wave signal generator (0.25–20 GHz, KeySight Technologies N5173B) [22]. For selected frequency regions (i.e. below 80 GHz and in the 120–200 GHz interval), we have instead employed Gunn oscillators (Farran and Carlstrom) phase-locked to a suitable harmonic of a cm-wave reference signal [21]. A 10 MHz Rb atomic clock provided standard frequency for improved accuracy and stability.

The spectra were generally recorded at room temperature, using the HC_3N sample at a static pressure of 3–10 μbar. For a restricted set of measurements, in the 250–300 GHz frequency range, we employed a hot sample with the aim of enhancing the signal of the rotational transitions belonging to the fundamental stretching states and their lowest combinations with the v_7 vibration. In such cases, vapors of HC_3N were flown through a 5 cm diameter, 2 m long, quartz cell sealed with high-density polyethylene windows placed in the heating zone of a tubular oven (Carbolite) [15]. A steady, slow flow at a pressure of ∼ 3 μbar were maintained by continuously pumping the sample through the cell kept at a temperature of 1000 °C.

3. Observed spectra

3.1. HC_3N IR spectrum

Cyanoacetylene is a linear molecule with seven IR active vibrational normal modes: they are ordered with decreasing energy: four are stretchings (ν_1, ν_2, ν_3, ν_4; Σ symmetry) and three are doubly-degenerate bendings (ν_5, ν_6, ν_7; Π symmetry). The vibrational energy levels of HC_3N are depicted in Fig. 1, while the appearance of the infrared spectra is depicted sideways on the left. The levels drawn with solid gray lines have already been considered in our previous works [3,6], whereas the ones targeted by the present investigations are plotted using solid blue lines. They are: the $v_5 = 2$ and $v_7 = 6$ overtones, and the $(v_4 = 1, v_7 = 2)$, $(v_5 = 1, v_7 = 3)$, $(v_6 = 2, v_7 = 2)$, $(v_2 = 1, v_7 = 2)$, and $(v_3 = 1, v_7 = 2)$ combination states. Experimental information on the energy position of these vibrational states has been obtained through the analysis of 11 new bands. Furthermore, we collected new data for six bands which were previously investigated in Ref. [6], with the aim of enlarging the data sets and improving the analysis. All these data are summarized in Table 1 and described in details in the following subsections.

3.1.1. The 1200–1400 cm^{-1} interval, the $2\nu_5$ band

This spectral window is dominated by the very strong $2\nu_5$ overtone band, which shows a $\Sigma - \Sigma$ structure. Highly-accurate line positions for $2\nu_5$ transitions up to $J \sim 80$ have been retrieved from a low pressure (1 μbar) spectrum, while a higher pressure acquisition (100 μbar) was used for higher J transitions. The same region had been studied in the past by Yamada et al. [14]; our reinvestigation is aimed at collecting an extensive data set at the maximum possible resolution to accurately model the various anharmonic perturbations. In fact, anomalies in the spectral pattern become evident around $J = 70$ (∼ 1292 cm^{-1} in the P-branch and 1335 cm^{-1} in the R-branch), where the $v_5 = 2$ upper level cross with the interacting $(v_4 = 1, v_7 = 2)$ combination. As a result, transitions in the $J = 65 - 75$ range belonging to the perturbation-allowed $\nu_4 + 2\nu_7$ band are present, embedded in the very intense pattern of the $2\nu_5$ band. All these features were already reported in Ref. [14], where a partial analysis was also attempted. However, the lack of a reliable and independent energy value for the $(v_4 = 1, v_7 = 2)$ level and the neglecting of other weaker interactions prevented a comprehensive modeling of the complete resonance network. Several other line sequences, attributable to the ν_7-associated hot bands, are also clearly visible, but they were not analyzed in the present work.

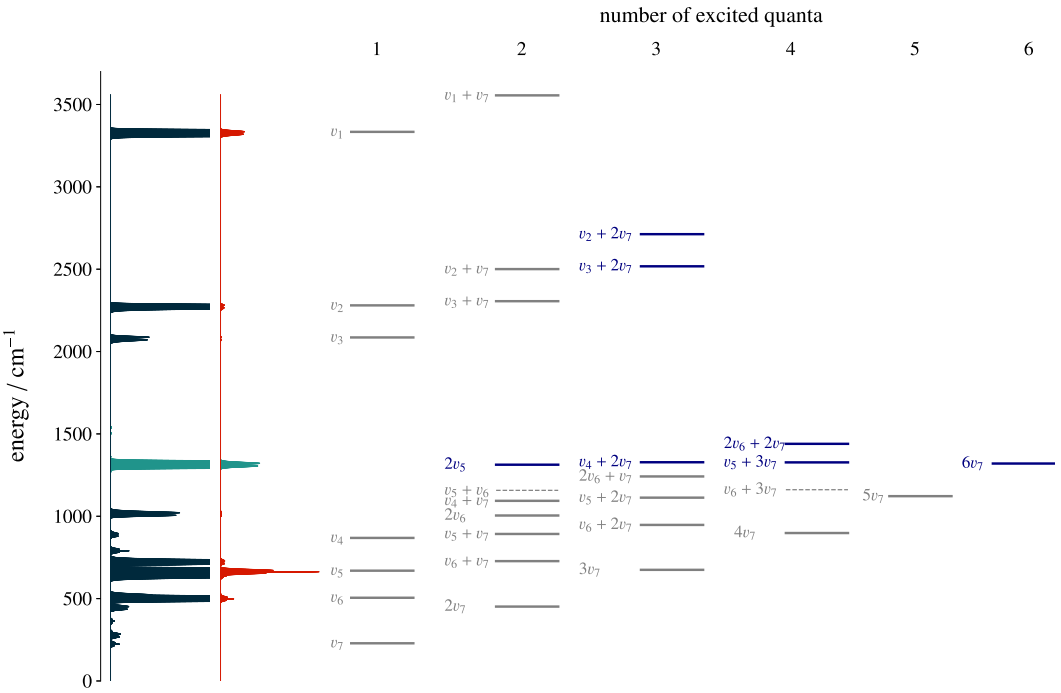

Fig. 1. Schematic representation of the vibrational energy manifold of HC_3N (complete below 1500 cm^{-1}). The states investigated in this work are drawn in blue solid lines. Gray dashed lines indicate the levels not considered in the present analysis. On the left, the appearance of the vibrational spectrum of HC_3N is depicted sideways adopting two different normalization factors. The intensity of the red trace is adjusted to show the prominent ν_1, ν_5, and ν_6 bands, whereas the dark blue spectrum is expanded 50 times in order to show the weaker bands. The $2\nu_5$ overtone, studied in the present work is highlighted in green.

Table 1
Ro-vibrational bands of HC_3N recorded and analyzed in this work.

Band[a]	Sub-bands	Freq. range (cm^{-1})	$J_{min} - J_{max}$	No. of lines	σ[b] (10^{-3}cm^{-1})	rms[c]
newly studied						
$2\nu_5^*$	$\Sigma^+ - \Sigma^+$	1279–1350	0–115	229	0.2/0.3[d]	0.83
$2\nu_5 - \nu_5$	$\Sigma^+ - \Pi$, $\Delta - \Pi$	620–686	1–89	339	0.3	0.73
$\nu_4 + 2\nu_7^*$	$\Sigma^+ - \Sigma^+$	1290–1338	62–80	31	0.4	0.63
$\nu_4 + 2\nu_7 - 2\nu_7$	$\Sigma^+ - \Sigma^+$, $\Delta - \Delta$	847–884	2–79	264	0.4	0.88
$\nu_4 + 2\nu_7 - (\nu_6 + 2\nu_7)$	$\Sigma^+ - \Pi$, $\Delta - \Pi$, $\Delta - \Phi$	347–386	2–67	394	0.3	0.90
$2\nu_6 + 2\nu_7 - 2\nu_7$	$\Sigma^+ - \Sigma^+$, $\Delta - \Delta$	992–1036	0–77	265	0.4	0.66
$2\nu_6 + 2\nu_7 - (\nu_6 + \nu_7)$	$\Sigma^+ - \Sigma^+$, $\Delta - \Delta$	717–759	5–70	159	0.3	1.41
$\nu_5 + 3\nu_7 - 2\nu_7$	$\Sigma^+ - \Sigma^+$, $\Delta - \Delta$	880–909	5–67	231	0.4	0.83
$6\nu_7 - 5\nu_7$	H – I	208–244	8–59	61	0.3	0.50
$\nu_2 + 2\nu_7 - 2\nu_7{}^*$	$\Sigma^+ - \Sigma^+$, $\Delta - \Delta$	2238–2290	0–91	315	0.5	0.71
$\nu_3 + 2\nu_7 - 2\nu_7{}^*$	$\Sigma^+ - \Sigma^+$, $\Delta - \Delta$	2049–2094	2–77	262	0.5	1.42
extended/revised						
$\nu_1{}^*$	$\Sigma^+ - \Sigma^+$	3295–3356	0–105	204	0.5	0.96
$\nu_2{}^*$	$\Sigma^+ - \Sigma^+$	2232–2297	0–105	192	0.4	0.92
$\nu_3{}^*$	$\Sigma^+ - \Sigma^+$	2045–2105	0–100	195	0.4	0.81
$\nu_1 + \nu_7 - \nu_7{}^*$	$\Pi - \Pi$	3298–3351	1–87	319	0.5	0.77
$\nu_2 + \nu_7 - \nu_7{}^*$	$\Pi - \Pi$	2233–2296	1–104	313	0.4	1.00
$\nu_3 + \nu_7 - \nu_7{}^*$	$\Pi - \Pi$	2048–2099	1–86	304	0.4	0.92

[a] Asterisks mark bands included in the HITRAN2024 release [23].
[b] Estimate of the experimental uncertainty.
[c] Dimensionless root mean square deviation of the global fit.
[d] 0.2×10^{-3} cm^{-1} for the 2 μbar spectrum and 0.3×10^{-3} cm^{-1} for the 100 μbar spectrum.

3.1.2. The 800–1050 cm^{-1} interval, hot bands in the ν_4 / $\nu_5 + \nu_7$ / $2\nu_6$ region

This interval has been newly recorded at relatively high pressure (100 μbar), thus enabling the identification of some weak hot bands that provided information about the energy of the ($v_4 = 1, v_7 = 2$), ($v_6 = 2, v_7 = 2$), and ($v_5 = 1, v_7 = 3$) levels. The ν_4 fundamental and the $\nu_5 + \nu_7$ combination bands (enhanced by the resonance) are located at ~ 885 cm^{-1} with partially overlapping rotational structures. Their first ν_7-associated hot bands had been already analyzed earlier [6]; here, we were able to assign the $\Sigma^+ - \Sigma^+$ and $\Delta - \Delta$ components of the $\nu_4 + 2\nu_7 - 2\nu_7$ and $\nu_5 + 3\nu_7 - 2\nu_7$ hot bands. The $2\nu_6$ overtone is located at higher wavenumbers (998 cm^{-1}), and its $2\nu_6 + \nu_7 - \nu_7$ hot band was already well characterized [6]. The identification of the line sequences corresponding to the $\Sigma^+ - \Sigma^+$ and $\Delta - \Delta$ sub-bands of the $2\nu_6 + 2\nu_7 - 2\nu_7$ hot band was then accomplished in a straightforward way.

3.1.3. The 600–750 cm^{-1} interval, hot bands in the ν_5 and $\nu_6 + \nu_7$ region

The ν_5 fundamental at 663 cm^{-1} is the strongest feature in the HC_3N IR spectrum and its hot-band manifold is particularly rich. A couple of ν_7-associated hot bands have been already studied in our previous

work [6], but many other line sequences are clearly discernible. Among them, we identified the $\Sigma^+ - \Pi$ and $\Delta - \Pi$ components of the $2\nu_5 - \nu_5$ hot band, which provides direct information on the energy position of the ($v_5 = 2, |l_5| = 2$) sub-level, not directly involved in the $2\nu_5$ fundamental. The $\nu_6 + \nu_7$ combination, located at the 720 cm^{-1}, and its ν_6- and ν_7–associated hot bands have been analyzed earlier [3,6]. In the present work, we assigned additional line sequences belonging to the $2\nu_6 + 2\nu_7 - (\nu_6 + \nu_7)$ hot band ($\Sigma^+ - \Sigma^+$, $\Delta - \Delta$).

3.1.4. The 200–400 cm^{-1} interval, hot bands in the ν_7 and $\nu_4 - \nu_6$ region

Far infrared data, collected in the course of previous studies, provided additional experimental information for the ($v_4 = 1, v_7 = 2$) combination, together with a direct determination of the vibrational energy of the highly excited $\nu_7 = 6$ bending state. The region of the lowest ν_7 fundamental (~ 220 cm^{-1}) is characterized by a high density of lines because of the complex structure of its hot bands, many of which involve bend-bend combinations and overtones. Despite the spectral congestion, we were able to successfully identify *ca.* 60 lines belonging to the H – I sub-band of the $6\nu_7 - 5\nu_7$ hot band. These transitions connect the ($v_7 = 6, |l_7| = 6$) and ($v_7 = 5, |l_7| = 5$) sub-levels. Their $e - f$ splitting is not resolvable under our experimental conditions, and thus they appear as blended lines with twice the computed intensity. The anharmonic interactions present in HC_3N vibrational manifold also enhance the $\nu_4 - \nu_6$ difference band, which is clearly visible at ~ 345 cm^{-1}. The $\nu_4+2\nu_7-(\nu_6+2\nu_7)$ band exhibits several sub-bands, among which we could identify the $\Sigma^+ - \Pi$ and the $\Delta - \Phi$ PQR-branches.

3.1.5. The 2000–3500 cm^{-1} interval, the stretching zone

The HC_3N stretching fundamentals are located in the upper part of the MIR spectrum at 2079 cm^{-1} (ν_3), 2274 cm^{-1} (ν_2), and 3327 cm^{-1} (ν_1). The whole interval was recorded by Jiang et al. [15] in the course of a study targeting the DC_3N IR spectrum. Since the parent species was also present as a side-product, the three ν_1, ν_2, and ν_3 fundamental bands of HC_3N and their corresponding hot bands originating from the $v_7 = 1$ bending state were also analyzed in that work. In the present study, we extended the spectroscopic investigation of the stretching fundamentals to their second most intense hot bands, which originate from the $v_7 = 2$ overtone state. Additionally, due to the higher sensitivity of the data collected at SOLEIL, we were able to significantly enlarge the data set for the previously observed bands [15], reaching $J_{max} \sim 105$.

We were able to identify the $\Sigma^+ - \Sigma^+$ and $\Delta - \Delta$ sequences of the $\nu_2+2\nu_7-2\nu_7$ and of the $\nu_3+2\nu_7-2\nu_7$ assigning 315 and 262 transitions, respectively. We could also pinpoint some short sequences of lines belonging to the $\nu_1+2\nu_7-2\nu_7$ band, but their trends are highly perturbed because of multiple accidental resonances, thus a complete analysis was not attempted. In fact, the ν_1 fundamental and its ν_7-associated hot bands show signs of perturbations: localized avoided crossings appear at $J \sim 43$ for the ν_1 fundamental, and at $J \sim 30$ and $J \sim 88$ for the $\nu_1 + \nu_7 - \nu_7$ hot band. Such anomalies, which had not been modeled in Ref. [15], have been explicitly treated in the present analysis.

3.2. HC_3N rotational spectrum

A comprehensive investigation of the rotational spectrum of HC_3N has been reported in a couple of recent papers [3,6]. These studies provided a detailed characterization of all the vibrational states below 1300 cm^{-1}, plus a few excited states with energies between 2075 and 3550 cm^{-1}. Here, we have recorded new mm- and submm-wave spectra for five vibrational states located between 1320 and 1430 cm^{-1}: they are $v_5 = 2$, ($v_4 = 1, v_7 = 2$), ($v_6 = 2, v_7 = 2$), ($v_5 = 1, v_7 = 3$), and $v_7 = 6$. These states constitute an interacting polyad with various close near-degeneracies, thus producing striking anomalies on the corresponding l-type spectral patterns. For this reason, we have made an attempt to record all the experimentally accessible transitions from 60 to 500 GHz with basically no gaps. Particular care has been exerted at covering the frequency regions where level crossings occur and the lines belonging to the involved states exhibit prominent deviations from the predicted unperturbed positions. These regions are at $J = 6$ (~ 64 GHz), $J = 28$ (~ 264 GHz), and $J = 48 - 55$ (446–510 GHz).

Additional measurements have been performed by using a hot sample (1000 °C), with the aim of detecting pure rotational transitions belonging to the high-energy stretching states. We targeted the 250–300 GHz frequency interval where signals due to the $v_3 = 1$, $v_2 = 1$, and $v_3 = v_7 = 1$ states could be actually identified. These measurements provided extra precision for the rotational parameters of these high-energy states, usually determined solely from infrared data. The summary of the pure-rotational data collected and analyzed in the present work is reported in Table 2.

3.3. HC_4H IR spectrum, the ν_4 band

Diacetylene is a linear centrosymmetric molecule with two equivalent hydrogen nuclei and two pairs of equivalent carbon nuclei which are interchanged by the C_2/i symmetry operations. The ro-vibrational states can thus be labeled according to the inversion and rotational parity and shows a 1:3 spin statistical weight ratio. Table 3 summarizes the spin multiplicity rules.

Diacetylene possesses nine vibrational normal modes: five stretching modes of Σ symmetry and four doubly degenerate bending modes of Π symmetry. Because of its symmetry, only four of these modes are infrared active. Among them, the asymmetric C–H stretching vibration ν_4 (Σ_u^+) is particularly intense and its fundamental band at ~ 3333 cm^{-1} represents one of the most prominent features of the entire IR spectrum of HC_4H.

The ν_4 fundamental exhibits a $\Sigma - \Sigma$ ro-vibrational structure, characterized by P- and R-branches only. As required by nuclear-spin statistics, the rotational line intensities display the expected 1:3 alternation. The overall appearance of the ν_4 band is regular at low and intermediate J values; however, starting at $J \sim 60$, pronounced anomalies become evident in both the line positions and their relative intensities (see Fig. 2). These irregularities arise from strong anharmonic interactions between the $v_4 = 1$ excited state and several nearby dark states, which produce localized perturbations and avoided crossings. While the most conspicuous effects occur at $J = 60$ and $J = 66$ as reported by Guelachvili et al. [9], large deviations persist well into the higher J region, in particular around $J = 84$ and $J = 104$.

The ν_4 band has been the subject of several previous high-resolution investigations carried out under different experimental conditions, ranging from room-temperature Fourier-transform absorption spectroscopy [9,24] to discharge experiments in supersonic-jet expansion, coupled with sub-Doppler difference-frequency techniques [25] or continuous-wave cavity ring-down spectroscopy [13]. Despite these numerous studies, the ro-vibrational analyses performed so far have systematically neglected the perturbations caused by the manifold of interacting dark states. As a consequence, spectral assignments are limited to $J \leq 83$ and the observed line positions are not reproduced within experimental accuracy for J values above 40.

In the present work, by exploiting the high sensitivity of the SOLEIL synchrotron source, we have recorded three spectra at different pressures in the ν_4 region and achieved a substantial extension of the ro-vibrational assignment. Transitions have been assigned up to $J = 115$ in the R-branch and up to $J = 98$ in the P-branch (the lower J coverage reached in the P-branch is due to the spectral congestion affecting the corresponding low-frequency side of the fundamental). Unlike previous analyses, the present treatment explicitly includes the anharmonic interactions between the $v_4 = 1$ level and four nearby dark states. Furthermore, several short sequences of transitions that borrow intensity through state mixing have been identified and incorporated into the global data set.

Table 2
Rotational transitions of HC_3N recorded in this work.

State	Freq. range (GHz)	J max	No. of lines	rms[a]
$v_4 = 1, v_7 = 2$	64–529	57	192	0.86
$v_5 = 2$	64–527	57	136	0.90
$v_6 = 2, v_7 = 2$	92–515	55	296	0.70
$v_5 = 1, v_7 = 3$	64–523	55	361	0.93
$v_7 = 6$	65–528	56	261	0.90
inter-state	64–513	54	20	0.93
$v_2 = 1$	253–308	33	6	0.52
$v_3 = 1$	253–327	35	8	0.68
$v_3 = v_7 = 1$	254–327	35	17	1.01

[a] Dimensionless root mean square deviation of the global fit.

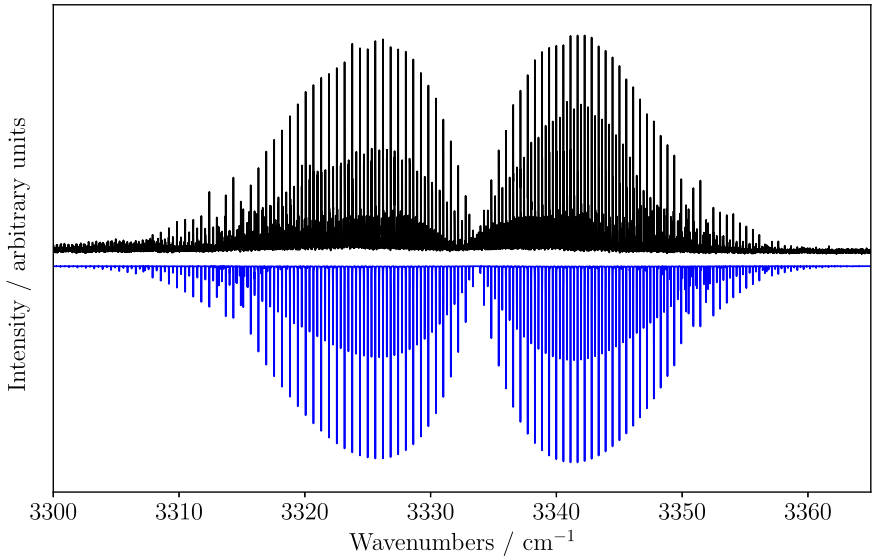

Fig. 2. Recording (*black trace*) of the ν_4 band of HC_4H, together with a simulated spectrum (*blue trace*, reversed) computed using the spectroscopic constants of Table 9. Anomalies in both the intensities and line positions are visible in the high J region of either branches. The band shows the typical 1:3 spin–statistics alternation. Both intensity scales are normalized.

Table 3
Spin statistical weights of the ro-vibrational levels of diacetylene.

Inversion parity	parity label	even J	odd J
g	e	1	3
	f	3	1
u	e	3	1
	f	1	3

4. Analysis and results

The ro-vibrational energy terms of HC_3N and HC_4H have been computed following the approach described in detail by Bizzocchi et al. [3]. Briefly, we set a linear molecule effective Hamiltonian as a sum of a ro-vibrational ($\tilde{H}_{\rm rv}$) and a l-type interaction ($\tilde{H}_{l\text{-type}}$) terms, plus an additional contribution ($\tilde{H}_{\rm res}$) accounting for the various anharmonic resonances:

$$\tilde{H} = \tilde{H}_{\rm rv} + \tilde{H}_{l\text{-type}} + \tilde{H}_{\rm res}\,. \tag{1}$$

$\tilde{H}_{\rm rv}$ is diagonal in all quantum numbers, whereas $\tilde{H}_{l\text{-type}}$ gives rise to several off-diagonal matrix elements with $\Delta k = 0, \pm 2, \pm 4$ ($k = \sum_t l_t$). $\tilde{H}_{\rm res}$ contains terms connecting the sub-blocks of the nearly-degenerate, interacting vibrational states. The reader is referred to Ref. [3] for the complete expressions of all the Hamiltonian terms.

The main interaction scheme that is effective in the HC_3N vibrational manifold has been described previously [3,6]. Basically, two features rule: (*i*) the interaction between $v_5 = 1$ and $v_7 = 3$, and (*ii*) the $(v_4 = 1) \sim (v_6 = 2) \sim (v_5 = v_7 = 1) \sim (v_7 = 4)$ cluster of levels. From these, an infinite sequence of polyads located at increasing energy can be generated by adding one or more quanta to the base level schemes. Eventually, these two series of resonance systems become entangled by raising in the vibrational energy manifold, because of the link provided by common levels [6]. In fact, by adding a v_5 quantum to (*i*) and two v_7 quanta to (*ii*), the two systems wrap around the $(v_5 = 1, v_7 = 3)$ level, thus generating a pentad of interacting states located at ca. 1350 cm^{-1}. They are $v_5 = 2$, $(v_4 = 1, v_7 = 2)$, $(v_6 = 2, v_7 = 2)$, $(v_5 = 1, v_7 = 3)$, and $v_7 = 6$. This resonance network has been analyzed in the present work and a graphical representation of the energy level positions and the main interactions is shown in Fig. 3. The resonance Hamiltonian $\tilde{H}_{\rm res}$ used here contains the terms $\tilde{H}_{30}$, $\tilde{H}_{32}$, $\tilde{H}_{40}$, $\tilde{H}_{42}$, $\tilde{H}_{50}$, and $\tilde{H}_{52}$, already described in Refs. [3,6].[2] In addition, two new terms, namely $\tilde{H}_{50}+\tilde{H}_{52}$, had to be included in the ro-vibrational energy calculations to take into account the quartic interactions between the $(v_5 = 2)$ overtone and the $(v_4 = 1, v_7 = 2)$ combination states:

$$\begin{aligned}\left\langle v_4, v_5^{l_5}, v_6^{l_6}, v_7^{l_7}; J, k \middle| \tilde{H}_{50} + \tilde{H}_{52} \middle| v_4 + 1, (v_5 - 2)^{l_5}, v_6^{l_6}, (v_7 + 2)^{l_7}; J, k \right\rangle \\ = \frac{\sqrt{2}}{4}\left[C_{50a}^{(45577)} + C_{50aJ}^{(45577)} J(J+1)\right] \\ \times \left\{(v_4+1)(v_5 \pm l_5 + 2)(v_5 \mp l_5 + 2)(v_7 \pm l_7 + 2)(v_7 \mp l_7 + 2)\right\}^{1/2}\,,\end{aligned} \tag{2}$$

[2] The Hamiltonian terms are labeled as $\tilde{H}_{mn}$, where m and n are the total degree of the vibrational and rotational operators, respectively.

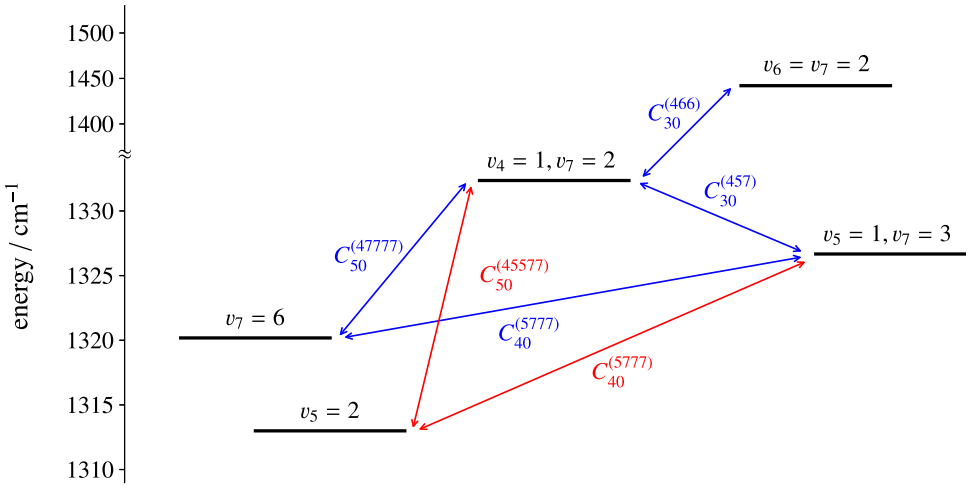

Fig. 3. Vibrational energy diagram for the interacting states $v_5 = 2$, $(v_4 = 1, v_7 = 2)$, $(v_6 = 2, v_7 = 2)$, $(v_5 = 1, v_7 = 3)$, and $v_7 = 6$ of HC_3N. Thin arrows indicate the $\Delta k = 0$ vibrational couplings taken into account.

$$\left\langle v_4, v_5^{l_5}, v_6^{l_6}, v_7^{l_7}; J, k \middle| \tilde{H}_{50} \middle| v_4 + 1, (v_5 - 2)^{l_5 \mp 2}, v_6^{l_6}, (v_7 \pm 2)^{l_7 \pm 2}; J, k \right\rangle = \frac{\sqrt{2}}{4} C_{50b}^{(45577)} \left\{ (v_4 + 1)(v_5 \pm l_5 - 2)(v_5 \pm l_5)(v_7 \pm l_7 + 2)(v_7 \pm l_7 + 4) \right\}^{1/2}, \quad (3)$$

$$\left\langle v_4, v_5^{l_5}, v_6^{l_6}, v_7^{l_7}; J, k \middle| \tilde{H}_{52} \middle| v_4 + 1, (v_5 - 2)^{l_5 \mp 2}, v_6^{l_6}, (v_7 \pm 2)^{l_7}; J, k \mp 2 \right\rangle = \frac{\sqrt{2}}{4} C_{52a}^{(45577)} \left\{ (v_4 + 1)(v_5 \pm l_5 - 2)(v_5 \pm l_5)(v_7 \mp l_7 + 2)(v_7 \mp l_7 + 2) \right\}^{1/2} \sqrt{f_{\mp 2}(J, k)}, \quad (4)$$

where the k-dependent term of the matrix element is given by (see Eqs. (3) of Ref. [3] for the general formula):

$$f_{\mp 2}(J, k) = [J(J+1) - k(k \mp 1)]\,[J(J+1) - (k \mp 1)(k \mp 2)]\,. \quad (5)$$

The $C_{50a}^{(45577)}$ and $C_{50b}^{(45577)}$ coefficients express the magnitude of the $\Delta k = 0$ interaction between the corresponding $l_t = 0$ and $l_t = 2^{ef}$ sub-levels, whereas the $C_{52a}^{(45577)}$ multiplies the $|\Delta k| = 2$ term coupling the $(v_4 = 1, v_7 = 2), l_7 = 0$ with the $v_5 = 2, l_5 = 2^{ef}$ sub-levels.

The ro-vibrational basis functions are chosen as product of one-/two-dimensional harmonic oscillator wave-functions and a rotational symmetric-top wave-function, $\left| v_s, v_5^{l_5}, v_6^{l_6}, v_7^{l_7}; J, k \right\rangle$, with $k = l_5 + l_6 + l_7$. In this notation, v_s summarizes the stretching mode vibrational quantum numbers v_1, v_2, v_3 and v_4. Symmetry-adapted basis functions are then obtained by the Wang-type linear combinations [26]:

$$\left| v_s, v_5^{l_5} v_6^{l_6}, v_7^{l_7}; J, k \right\rangle_{e/f} = \frac{1}{\sqrt{2}} \left\{ \left| v_s, v_5^{l_5}, v_6^{l_6}, v_7^{l_7}; J, k \right\rangle \pm (-1)^k \left| v_s, v_5^{-l_5}, v_6^{-l_6}, v_7^{-l_7}; J, -k \right\rangle \right\}, \quad (6a)$$

$$\left| v_s, 0^0 0^0, 0^0; J, 0 \right\rangle_e = \left| v_s, 0^0, 0^0, 0^0; J, 0 \right\rangle\,. \quad (6b)$$

For even (odd) value of k, the upper and lower signs $(\pm)$ correspond to the e (f) and f (e) wave-functions [27], respectively. For Σ states $(k = 0)$, the first non-zero l_t is chosen positive.

In the case of HC_4H, the effective Hamiltonian used is considerably simpler because the present work focuses on a single vibrational band and does not aim at a global analysis of the entire vibrational manifold. In particular, since both the lower and upper states of the ν_4 fundamental possess Σ symmetry, the $\tilde{H}_{l\text{-type}}$ term does not appear at all in the Hamiltonian. Moreover, given the high energy of the $v_4 = 1$ level and the extremely dense vibrational structure in this region, it is not possible to unambiguously identify all the states interacting with $v_4 = 1$. For this reason, the operators appearing in the $\tilde{H}_{\text{res}}$ term have been introduced in a simplified and generic form, without specifying the exact vibrational nature of the perturbing states. Further details on this are provided in Section 4.3 and in Eq. (8).

4.1. ^{14}N-quadrupole coupling in $k = 6$ lines of HC_3N

A few low-J rotational transitions recorded for HC_3N in the $v_7 = 6$ vibrationally excited states show evidences of hyperfine splitting due to the ^{14}N-quadrupole coupling ($I_N = 1$). For the $v_7 = 6$ overtone states, values of l_7 up to 6 are generated, which correspond to $k = 6$ in the rotational wavefunction allowed by the linear molecule isomorphic Hamiltonian [28,29]. The hyperfine splitting is known to be small and usually resolvable only for low J lines, as the corresponding hyperfine components rapidly collapse for increasing J. On the other hand, the hyperfine splittings increase with increasing values of the k quantum number, that labels the projection of the rotational angular momentum on the molecular axis.

For the $v_7 = 6$ rotational lines, the quadrupole splitting is large enough to produce detectable effects for the $J < 10$. An example is illustrated in Fig. 4 showing the recording of the $v_7 = 6$, $J = 7 \leftarrow 6$ transitions of HC_3N together with the computed stick spectra that illustrate the effect of the hyperfine interaction. For the $k = 0$ and $k = 2$ components the coupling is less pronounced and the lines are only slightly broadened; the $k = 4$ clearly appears as a doublet, while $k = 6$ show a more complex pattern partially overlapped with the $k = 2^f$ component. The simulated hyperfine spectrum plotted as the red stick spectrum in Fig. 4 has been computed using the rotational and ro-vibrational parameters of Tables 4–5, plus the ^{14}N-coupling hyperfine constants derived from the results of the molecular beam experiments by DeLeon and Muenter [30].

Using cartesian tensor notation, the hyperfine term of the Hamiltonian reads as:

$$\tilde{H}_{\text{hfs}} = e\mathbf{Q} : \mathbf{q} + \mathbf{I} \cdot \mathbf{C} \cdot \mathbf{J}\,. \quad (7)$$

The first contribution is the nuclear quadrupole coupling and is expressed as dyadic product of the nuclear quadrupole tensor $e\mathbf{Q}$, where e is the elementary charge, and the electric field gradient tensor $\mathbf{q}$. The second term describes the weak magnetic spin–rotation interaction ($\mathbf{C}$ tensor) between the nuclear spin and the rotational angular momentum. For $k \neq 0$ states, the electric field gradient tensor q is anisotropic, thus two hyperfine quantities are needed to fully model the quadrupole interaction; they are eQq_{aa} and $eQ(q_{bb} - q_{cc})$ [30]. Because of its much smaller magnitude, the ^{14}N spin–rotation coupling have been modeled using a unique scalar coefficient (C_N) and the effect produced by the H nucleus has been neglected.

To take into account the resonance effects, a set of hyperfine constants has been computed for each state of the polyad considering the relevant vibrational dependence. The computed splittings were then

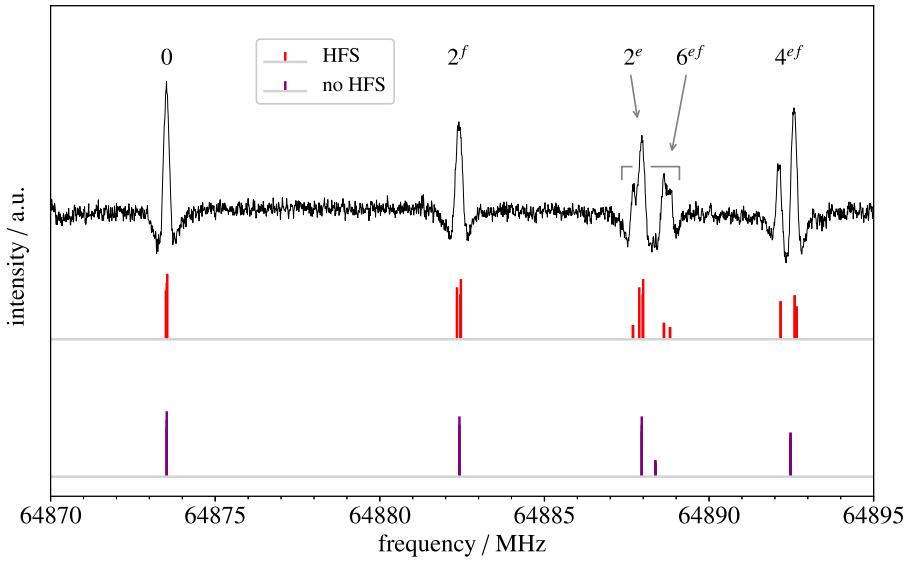

Fig. 4. Recorded spectrum (*black trace*) of the HC_3N, $J = 7 \leftarrow 6$ transition belonging the $v_7 = 6$ overtone state. The k labeling is marked on the top of each line. The red stick spectrum indicates the positions and the relative intensities of the quadrupole components, whereas the purple stick spectrum plots the hypothetically hyperfine-free spectrum (see text for details).

used to retrieve, from the line showing resolvable quadrupole patterns, the hypothetically hyperfine-free transition which was then included in the global fit.

4.2. Resonance polyad of HC_3N

The analysis of the ro-vibrational data involving the five vibrational states of the resonance polyad has been conducted adopting the approach described in details in Refs. [3,6]. The overall data set comprises 1191 pure rotational transitions and 1973 infrared lines, which have been simultaneously analyzed in a least-squares fitting procedure. The different measurement precision (σ) of the various data has been taken into account by adopting, for each datum, a weighting factor, $w = 1/\sigma^2$. The σ values for the new infrared data measured in this work are reported in the rightmost column of Table 1. For our, newly measured rotational lines a unique value of $\sigma = 30$ kHz has been used, whereas previously reported data [31] for the $(v_4 = 1, v_7 = 2)$ and $v_5 = 2$ states were inserted in the fit with the weights provided in the original paper.

Because of the multiple l-type resonance effects occurring among the sub-levels of the excited states considered, intricate spectral patterns have been generally observed. An example is given in Fig. 5 showing an excerpt of the rotational spectrum of HC_3N around 110 GHz. The figure inset depicts the inner part of this spectral range where we have assigned lines for the $(v_6 = v_7 = 2)$, $(v_5 = 1, v_7 = 3)$, and $(v_6 = 1, v_7 = 3)$ combination states (the latter is not presented in this work).

The analysis of the experimental frequencies provided energy positions and effective spectroscopic constants for the five states, namely: $v_5 = 2$, $(v_4 = 1, v_7 = 2)$, $(v_6 = 2, v_7 = 2)$, $(v_5 = 1, v_7 = 3)$, and $v_7 = 6$, plus 20 interaction coefficients describing the various anharmonic resonances between nearly-degenerate vibrational states. Some constants could not be directly determined from the fit procedure and we thus had to adopt a number of suitable constraints. These values were derived from lower-excited states considering, whenever feasible, a linear dependence from the vibrational quantum numbers (see Ref. [3] for details).

The structure of the resonance system centered at 1300 cm^{-1} has been already introduced in Section 4. In such a coupling scheme, the main features are the cubic interactions which take place between the $(v_4 = 1, v_7 = 2)$ and the two $(v_6 = 2, v_7 = 2)$, $(v_5 = 1, v_7 = 3)$ bend–bend combinations. Remarkably, $v_5 = 2$ and $(v_5 = 1, v_7 = 3)$ states are also connected via a quartic interaction, and additional weak quintic resonances $(v_4 = 1, v_7 = 2) \sim v_5 = 2$ and $(v_5 = 1, v_7 = 3) \sim v_7 = 6$, complete the coupling network (see Fig. 3).

A conspicuous feature of the present resonance polyad is the close vicinity of the $(v_5 = 1, v_7 = 3)$, and the $v_7 = 6$ states. They are coupled by the $\tilde{H}_{40}$ Hamiltonian term with resulting perturbations affecting the Σ, Δ, and Γ sub-levels. Due to the complex energy manifold of the $(v_5 = 1, v_7 = 3)$ combination, several avoided crossings take place between its sub-levels and the ones of the $v_7 = 6$ overtone. Such features are illustrated by the reduced frequency plot shown in Fig. 6. The effects of these perturbations on the spectral patterns are apparent in the 50–55 J range (470–515 GHz) where multiple, almost exact, degeneracies occur between $k = 2^{ef}, 4^{ef}$ sub-levels, thus producing major displacement of the lines from their unperturbed positions. Furthermore, localized anomalies are exhibited by the spectra of the $v_5 = 2$ and the $(v_4 = 1, v_7 = 2)$ states at $J \sim 28$ and at $J \sim 71$ (this latter not covered by our measurements), and between $v_5 = 2$ and $(v_5 = 1, v_7 = 3)$ states at $J \sim 5$. There, large deviations from the regular, divergent trends generated by the l-type resonance effects are suggestive of the presence of anharmonic coupling between vibrational states. In some of the above mentioned cases, the ro-vibrational wave-functions involved in the interaction are mixed to such an extent that the assignment of a level to either of the two vibrational manifolds becomes arbitrary (see Ref. [6] for details about the assignment method adopted). As a result, new rotational lines, formally labeled as *inter-state*, appear by borrowing intensity from the regular transitions occurring within the two vibrational manifolds. These exotic lines are marked with a cross in Fig. 6, and are more easily detected for those J values at which the corresponding pair of levels becomes closely degenerate. Effects of the state-mixing is observable in the infrared spectrum too: Fig. 7 shows an excerpt of the R-branch of the $2\nu_5$ band, where an avoided crossing is visible. As a result, the lines belonging to the $\nu_4 + 2\nu_7$ combination gain enough intensity to become readily detectable in proximity of the avoided crossing.

We underline that the analysis of the resonance polyad has been carried out without any assumption on the energy position of the interacting levels. In this respect, the inclusion in the analysis of infrared data from the hot bands (summarized in Table 1) provided critical information on the absolute energy position of the various excited states. The network of resonances has been modeled with the terms described in Refs. [3,6] plus the ones reported here in Eqs. (2)–(4). The inclusion of high-order terms such as $\tilde{H}_{52}$, whose contribution is estimated to

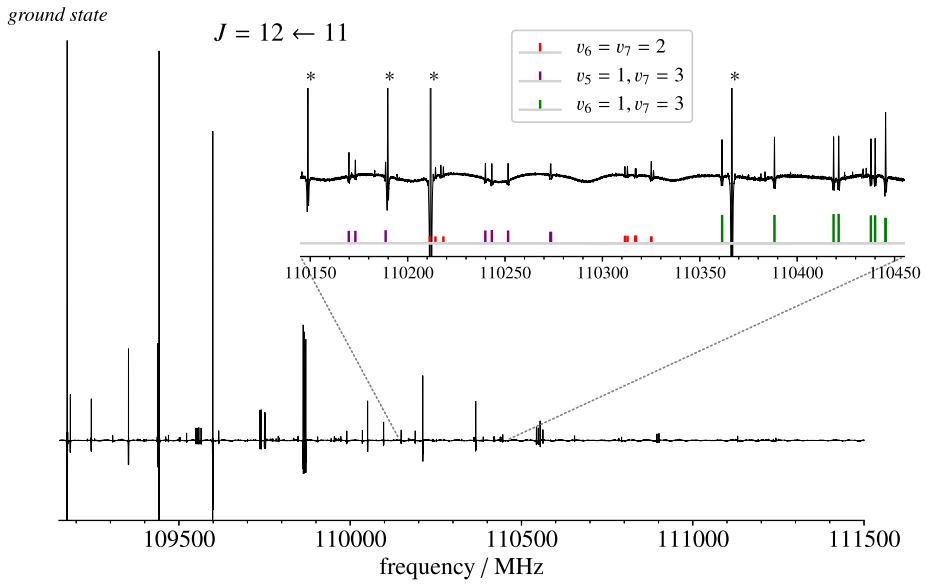

Fig. 5. Recorded spectrum of the $J = 12 \leftarrow 11$ transition of HC_3N. The strong ground state feature located at the leftmost plot position is saturated. The inset expands the frequency region where the spectral patterns of the ($v_6 = v_7 = 2$), ($v_5 = 1, v_7 = 3$) and ($v_6 = 1, v_7 = 3$) states are located. The predicted position and the relative intensity of the various components are indicated by the colored stick spectrum. The asterisks mark line belonging to low-lying vibrational satellites.

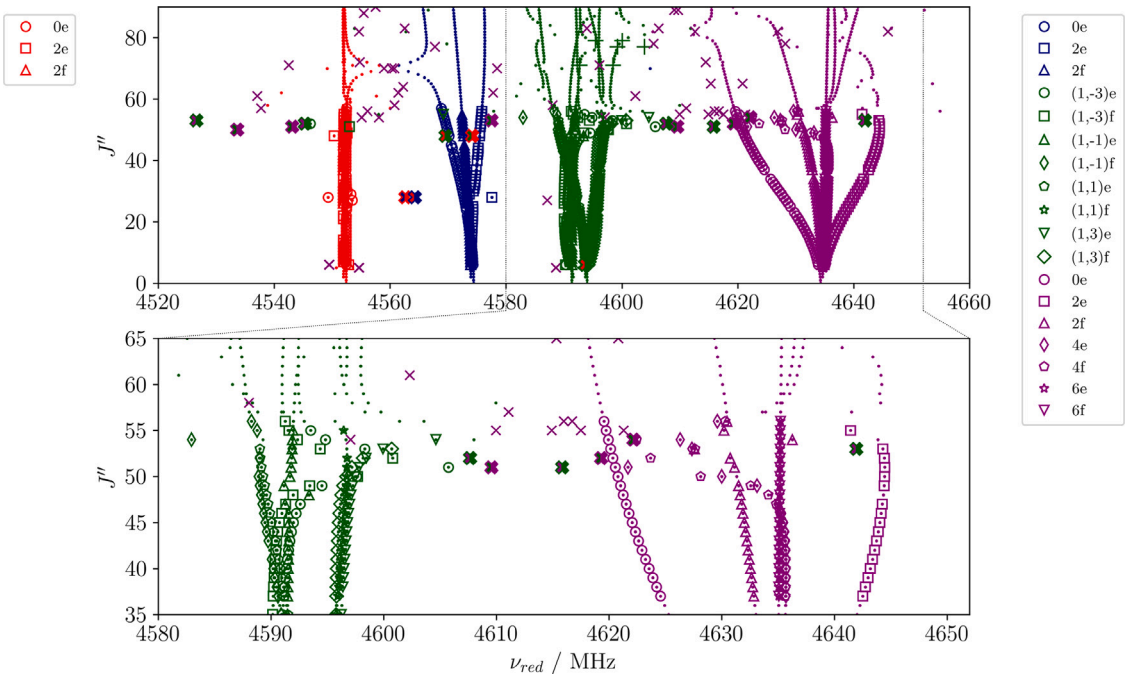

Fig. 6. Reduced frequency diagram for the $v_5 = 2$ (red symbols), ($v_4 = 1, v_7 = 2$) (blue symbols), ($v_5 = 1, v_7 = 3$) (green symbols), and $v_7 = 6$ (purple symbols) interacting states of HC_3N. The quantity plotted on the x-axis is $\nu_{red} = [\nu + 4D_0(J+1)^3]/2(J+1)$, where $D_0 = 0.5443$ kHz (ground-state value). Open symbols denote experimental values, whereas small dots indicate calculated values based on the parameters of Tables 4 and 5. Filled crosses label measured inter-state cross-over transitions, while the purple "times" symbols (×) are used for those predicted by the actual model. The "plus" signs (+) are employed for the ($v_5 = 1, v_7 = 3$) intra-state $(1,3)e/(1,-3)e$ cross-overs occurring at $J = 71$ and $J = 77$. The most perturbed transitions are labeled using the method implemented in the SPFIT code [32]. The bottom panel shows a detail of the upper plot in the ν_{red} range from 4580 to 4651 MHz.

be as small as $k^5\omega_{vib} \sim 0.03$ MHz [33], is justified by the presence of "exact" degeneracies occurring between $|\Delta k| = 2$ sub-levels and by the high precision of the rotational measurements used in the analysis. In fact, the final fit resulted in a weighted root-mean-square (rms) of $\sigma_w = 0.864$ thus validating that, on average, the totality of the analyzed data have been reproduced within the estimated experimental uncertainties. The complete list of the fitted transitions and their *obs-calc* residuals has been deposited as Supplementary Material.

Table 4
Spectroscopic constants derived for HC_3N for the level of the resonance polyad.

Constant	Unit	$v_5 = 2$	$v_4 = 1, v_7 = 2$	$v_6 = 2, v_7 = 2$	$v_5 = 1, v_7 = 3$	$v_7 = 6$
G_v	cm^{-1}	1312.99236 (12)	1332.5383 (11)	1435.1539 (20)	1321.96501 (59)	1320.18029 (19)
$x_{L(tt)}$	GHz	154.72789 (94)	...	6.64[a]	154.72792[a]	...
$x_{L(77)}$	GHz	...	22.4451 (88)	21.4835 (84)	21.49487 (52)	20.88179 (45)
$y_{L(77)}$	GHz	...	−1.955[a]	−1.955[a]	−1.955[a]	−0.0196 (82)
$x_{L(t7)}$	GHz	...	...	16.930 (15)	18.8729 (66)	...
r_{t7}	GHz	...	...	−14.075 (29)	8.130 (11)	...
r_{t7J}	kHz	...	...	−20.20 (57)	−73.81 (54)	...
r_{t7JJ}	Hz	...	...	1.60 (63)	1.02[a]	...
B_v	MHz	4552.38478 (19)	4566.5689 (24)	4596.727801 (19)	4593.97334 (65)	4635.50098 (19)
D_v	kHz	0.548116 (41)	0.60030 (11)	0.612270 (14)	0.616531 (32)	0.693971 (39)
H_v	mHz	0.0451 (31)	0.536[a]	0.2302[a]	0.1062[a]	0.3749[a]
L_v	nHz	−0.299[a]	−0.299[a]	−0.299[a]	−0.299[a]	−0.299[a]
$d_{JL(tt)}$	kHz	−112.422 (53)	...	12.32[a]	−112.422[a]	...
$h_{JL(tt)}$	Hz	−0.362 (13)	...	...	−0.363[a]	...
$d_{JL(77)}$	kHz	...	−25.702 (94)	−3.054 (62)	−15.499 (35)	−16.9081 (77)
$h_{JL(77)}$	Hz	...	0.0549[a]	−0.0549[a]	0.0160 (49)	0.1314 (16)
$l_{JL(77)}$	μHz	...	−3.956[a]	−3.956[a]	−3.576[a]	−2.438[a]
$d_{JL(t7)}$	kHz	...	...	52.428 (29)	1.81 (32)	...
$h_{JL(t7)}$	Hz	...	...	0.394 (74)	0.353 (25)	...
q_t	MHz	2.53861[a]	...	3.67226[a]	2.5862 (12)	...
q_{tJ}	Hz	−1.3352[a]	...	−2.4735[a]	−1.4395[a]	...
q_7	MHz	...	6.5759 (14)	6.6677 (16)	6.57403 (44)	6.655969 (99)
q_{7J}	Hz	...	−17.954 (88)	−17.39 (14)	−16.632 (41)	−17.378 (16)
q_{7JJ}	μHz	...	55.41[a]	55.41[a]	54.92[a]	52.36[a]
u_{77}	Hz	...	−0.11185[a]	−0.07002[a]	...	−0.0949 (11)
u_{t7}	Hz	...	...	−0.382[a]	0.739 (12)	...
q_{t77}	kHz	...	...	−4.9 (18)	−3.143 (30)	...
q_{tt7}	kHz	...	...	−1.22 (37)	...	...

Numbers in parentheses are one standard deviation in units of the last quoted digit.
[a] Assumed value (see text).

Table 5
Resonance parameters.

Interacting states	Parameter	Unit	Value
$(v_4 = 1, v_7 = 2) - (v_6 = 2, v_7 = 2)$	$C_{30}^{(466)}$	cm^{-1}	17.63941 (85)
	$C_{32}^{(466)}$	kHz	524.5 (94)
	$C_{30k}^{(466)}$	MHz	70.4 (33)
$(v_4 = 1, v_7 = 2) - (v_5 = 1, v_7 = 3)$	$C_{30}^{(457)}$	cm^{-1}	−2.3984 (20)
	$C_{32}^{(457)}$	kHz	−27.3 (11)
	$C_{30k}^{(466)}$	MHz	248.3 (59)
$(v_4 = 1, v_7 = 2) - (v_7 = 6)$	$C_{50}^{(47777)}$	MHz	2844.5 (15)
	$C_{40}^{(5777)}$	MHz	935.2 (28)
	$C_{40J}^{(5777)}$	MHz	−0.00449 (93)
	$C_{42a}^{(5777)}$	kHz	5.219 (54)
	$C_{42b}^{(5777)}$	kHz	−1.584 (33)
$(v_4 = 1, v_7 = 2) - (v_5 = 2)$	$C_{50a}^{(45577)}$	MHz	−1065 (22)
	$C_{50b}^{(45577)}$	MHz	−567.7 (27)
	$C_{50aJ}^{(45577)}$	MHz	−0.0185 (47)
	$C_{52a}^{(45777)}$	MHz	−0.0019 (10)
$(v_5 = 1, v_7 = 3) - (v_5 = 2)$	$C_{40}^{(5777)}$	MHz	−812.7 (42)
	$C_{42a}^{(5777)}$	KHz	−9.11 (71)
	$C_{42b}^{(5777)}$	kHz	−11.9 (45)

Numbers in parentheses are one standard deviation in units of the last quoted digit.

The optimized spectroscopic constants and resonance parameters determined for the levels included in the resonance polyad are reported in Tables 4 and 5. For the vibrational states below 1300 cm^{-1}, which are involved as lower states of the analyzed infrared bands, the spectroscopic parameters reported in Ref. [6] have been used.

4.3. Stretching bands of HC_3N

Compared to our previous study [6], here we have extended the investigation to two more hot bands: $\nu_2 + 2\nu_7 - 2\nu_7$ and $\nu_3 + 2\nu_7 - 2\nu_7$. In addition, significant improvement of the spectroscopic constants for the $v_2 = 1$, $v_3 = 1$, and $v_3 = v_7 = 1$ states has been provided by the

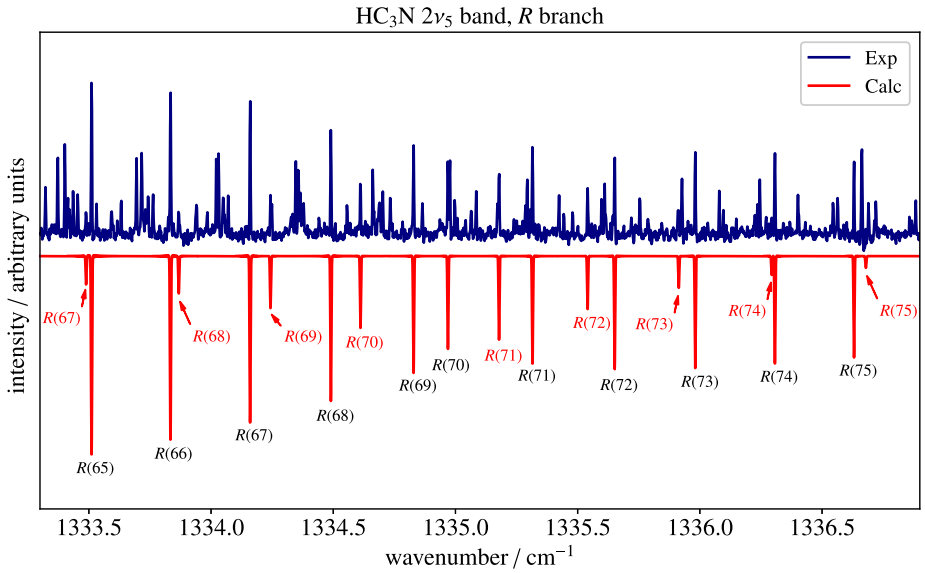

Fig. 7. Recording (*blue trace*) of a portion of the $2\nu_5$ band of HC_3N (R branch), together with a simulated spectrum (*red trace*, reversed) computed using the spectroscopic constants of Tables 4 and 5. The red labels indicate the assignments for the perturbation-allowed $\nu_4 + 2\nu_7$ combination band. Both intensity scales are normalized.

inclusion in the analysis of the high-precision rotational measurements carried out using the hot sample (see Section 2). In fact, the rotational parameters B_v, D_v, q_7, and q_{7J} have their standard uncertainties reduced up to one order of magnitude compared to previous results [6]. For the Δ states, $(v_3 = 1, v_7 = 2)$ and $(v_2 = 1, v_7 = 2)$, the anharmonicity constant $x_{(L77)}$ and the high-order parameter $d_{JL(77)}$ have been also determined. The optimized values for these quantities have then been used as constraints in the data sets of the corresponding Π states. The fit results are reported in Tables 6 and 7.

A careful examination of the spectral trends of the ν_1 system revealed minor anomalies in both P and R branches around $J \sim 48$ for ν_1 fundamental, and at $J \sim 30$ and $J \sim 88$ for the $\nu_1 + \nu_7 - \nu_7$ hot band. In all cases, irregular line intensities and positions were observed. The anomalies shown by the ν_1 band have been interpreted as due to an accidental degeneracies with an unknown Σ sub-level located $\approx 4\,\mathrm{cm}^{-1}$ below the $v_1 = 1$ state. This is referred as `dark1` state. As far as the $\nu_1 + \nu_7 - \nu_7$ hot bands is concerned, we postulate the existence of two perturbing Π sub-states placed $\approx 1\,\mathrm{cm}^{-1}$ (`dark2`) and $\approx 7\,\mathrm{cm}^{-1}$ (`dark3`) below the $v_1 = v_7 = 1$ state.

To model the observed spectral irregularities, we added into the resonance Hamiltonian [Eq. (1)] three further Fermi-type ($\Delta k = 0$) terms expressing the couplings: $v_1 = 1 \sim$ `dark1`, and $v_1 = v_7 = 1 \sim$ `dark2` $\sim$ `dark3`. The matrix elements have the form:

$$\langle v_1, v_7; J, k | \, \tilde{H}_{n0} \, | \, \mathtt{darkX}\,; J, k \rangle = C_{n0}^{(1\mathbf{q})} \,. \tag{8}$$

The symbols are adopted in coherence with the notation used in Eqs. (2)–(4) and in our previous work [3]: here, the general symbol n expresses the order in the vibrational operators contained in the $\mathbf{q} = rst\ldots$ unknown sequence of quanta. Besides the determinable C_{n0} terms, a few spectroscopic parameters have also been optimized for the dark states. They are: the vibrational energy (G_v), and the effective values of the rotational (B_v), and centrifugal distortion constants (D_v). Additionally, for the Π states, a fictitious l-type doubling constant (q_v) had also to be adjusted in order to model the $e - f$ sub-level separation of the perturbing states. The results of the analysis for $v_1 = 1$, $(v_1 = v_7 = 1)$, and the related dark states are reported in Tables 6–8. With the adoption of this treatment, 73 perturbed transitions (including 3 formally assigned to the unknown `dark1` state), which were previously excluded from the fit, could be successfully reproduced within experimental accuracy.

4.4. ν_4 band of HC_4H

Compared to earlier investigations of the ν_4 fundamental of diacetylene, in particular the high-resolution work of Guelachvili et al. [9] which has long served as the reference dataset, the present analysis achieved two major improvements. First, the ro-vibrational assignment has been extended up to $J = 115$, significantly enlarging the spectral coverage available for this band. Second, and more importantly, we have explicitly treated the anharmonic interactions between the $v_4 = 1$ state and four nearby dark states. These couplings, previously neglected in all analyses of ν_4, are responsible for several intensity- and frequency-anomalies observed at high J values. The inclusion of these interactions in the effective Hamiltonian was essential for reproducing the complex spectral behavior of the ν_4 band. With the adopted resonance scheme, both the line positions and their intensities are matched within the experimental accuracy, and our final fit shows a root-mean-square error of $5.6 \times 10^{-4}\,\mathrm{cm}^{-1}$, fully consistent with the uncertainty associated to our new measurements (the linewidth being approximately $6 \times 10^{-3}\,\mathrm{cm}^{-1}$).

The extended dataset and the explicit resonance treatment allowed us to determine reliable spectroscopic parameters for the $v_4 = 1$ state with high precision. In particular, the vibrational term value G_v, the rotational constant B_v, and the centrifugal-distortion constant D_v have been accurately derived; their values are listed in Table 9. The same Table also reports the G_v and B_v values, determined for the four dark states involved in the interaction network, together with the Fermi-type coupling parameters used to model their interactions with $v_4 = 1$. These terms play the same role as in the treatment of the HC_3N ν_1 system discussed in the previous section, and they are crucial for correctly describing the observed patterns. Our analysis also includes 15 ro-vibrational lines belonging to three of the four dark states.

5. Line list

The results of the ro-vibrational analyses presented here allowed for a major improvement of the rest-frequencies databases for HC_3N and HC_4H, both being notorious astrochemical tracers. More specifically, for cyanoacetylene we are now able to provide a significant integration to our previous linelist [6], also included in the HITRAN2020 edition of the database [34].

Table 6
Spectroscopic constants derived for HC_3N in stretching Σ states.

Constant	Unit	$v_3 = 1$	$v_2 = 1$	$v_1 = 1$	dark1
G_v	cm^{-1}	2079.305998 (34)	2273.994751 (35)	3327.369567 (64)	3324.288 (16)
B_v	MHz	4535.11723 (22)	4527.49587 (23)	4541.7897 (11)	4592.18 (25)
D_v	kHz	0.541259 (45)	0.538324 (36)	0.54116 (11)	0.54425[a]
H_v	mHz	0.0501[a]	0.0501[a]	0.0501[a]	
L_v	nHz	−0.299[a]	−0.299[a]	−0.299[a]	
$C_{n0}^{(1r)}$	MHz				639 (11)

Numbers in parentheses are one standard deviation in units of the last quoted digit.
[a] Kept fixed to the ground state value.

Table 7
Spectroscopic constants derived for HC_3N in Π, Δ stretching–bending combination states.

Constant	Unit	$v_3 = v_7 = 1$	$v_2 = v_7 = 1$	$v_3 = 1, v_7 = 2$	$v_2 = 1, v_7 = 2$
G_v	cm^{-1}	2298.788010 (26)	2493.659922 (43)	2517.487419 (76)	2712.556845 (66)
$x_{L(77)}$	GHz	21.4883[a]	21.5177[a]	21.48881 (72)	21.51769 (68)
$y_{L(77)}$	MHz	−1.955[a]	−1.955[a]	−1.955[a]	−1.955[a]
B_v	MHz	4549.73194 (20)	4541.98990 (75)	4564.3028 (20)	4556.4511 (12)
D_v	kHz	0.566533 (66)	0.562008 (80)	0.58863 (38)	0.58524 (17)
H_v	mHz	0.1084[a]	0.1084[a]	0.1638[a]	0.1638[a]
L_v	nHz	−0.299[b]	−0.299[b]	−0.299[b]	−0.299[b]
$d_{JL(77)}$	kHz	−10.23[a]	−9.35[a]	−10.23 (33)	−9.35 (28)
$h_{JL(77)}$	Hz	0.0361[a]	0.0361[a]	0.0549[a]	0.0549[a]
$l_{JL(77)}$	μHz	−4.33[a]	−4.33[a]	−3.96[a]	−3.96[a]
q_t	MHz	6.45563 (40)	6.65196 (96)	6.45563[a]	6.66753 (57)
q_{7J}	Hz	−14.32 (12)	−18.75 (13)	−14.32[a]	−18.75[a]
q_{7JJ}	μHz	56.55[a]	56.55[a]	55.41[a]	55.41[a]

Numbers in parentheses are one standard deviation in units of the last quoted digit.
[a] Assumed value, see text.
[b] Kept fixed to the ground state value.

Table 8
Spectroscopic constants derived for the perturbed $v_1 = v_7 = 1$ state of HC_3N.

Constant	Unit	$v_1 = v_7 = 1$	dark2	dark3
G_v	cm^{-1}	3548.405590 (67)	3547.33 (27)	3541.33 (17)
$x_{L(77)}$	GHz	21.8235[a]		
$y_{L(77)}$	MHz	−1.955[a]		
B_v	MHz	4556.2381 (15)	4614.2 (87)	4585.92 (66)
D_v	kHz	0.56451 (25)	0.56821[a]	0.56821[a]
H_v	mHz	0.1084[a]		
L_v	nHz	−0.299[a]		
$d_{JL(77)}$	kHz	−12.3148[a]		
$h_{JL(77)}$	Hz	0.03606[a]		
$l_{JL(77)}$	μHz	−4.33[a]		
q_t	MHz	6.5419 (18)	11.56 (68)	5.486 (27)
q_{7J}	Hz	−16.73 (34)	−16.2807[a]	−16.2807[a]
q_{7JJ}	μHz	56.55[a]		
$C_{n0}^{(1s)}$	MHz		951 (62)	
$C_{n0}^{(1t)}$	MHz			−3933 (29)

Numbers in parentheses are one standard deviation in units of the last quoted digit.
[a] Assumed value, see text.

Table 9
Spectroscopic constants derived for HC_4H[a].

Constant	Unit	$v_4 = 1$	dark1	dark2	dark3	dark4
G_v	cm^{-1}	3333.657928 (50)	3331.661 (10)	3327.289 (42)	3325.754 (80)	3329.6145 (41)
B_v	MHz	4382.6715 (11)	4399.059 (82)	4425.97 (28)	4415.93 (34)	4393.3629
D_v	kHz	0.46760 (11)	0.47037[b]	0.47037[b]	0.47037[b]	0.47037[b]
$C_{n0}^{(4r)}$	MHz		2952.7 (53)	2426.5 (56)	1992.3 (63)	709 (13)

Numbers in parentheses are one standard deviation in units of the last quoted digit.
[b] Ground state constants were fixed at $B_0 = 4389.298$ MHz and $D_0 = 0.47037$ kHz.
[b] Kept fixed to the ground state value.

It is to be pointed out that in the earlier release of HITRAN, no data were available for the 1270–1360 cm^{-1} wavenumber range, where the prominent $2\nu_5$ band is located. Thanks to the careful treatment of the anharmonic resonances involving $v_5 = 2$ overtone band, we have been able to compute a comprehensive list of rest-frequencies characterized by 1σ statistical uncertainties as low as 1×10^{-4} cm^{-1}. A small number of spectral features produced by the perturbation-allowed $\nu_4 + 2\nu_7$ band become clearly detectable in the most perturbed regions and are also included in the list.

The computation of the line strengths for the $2\nu_5$ band followed the same approach described by Tamassia et al. [6] (see Appendix A for details). The relevant Θ_5 intensity factor has been derived using the

absolute band intensity experimentally determined in Ref. [35]. The reported value has an uncertainty of about 5% ($70 \pm 3.5\,cm^{-2}\,atm{-}1$), which would translate to slightly larger uncertainty for individual ro-vibrational lines ($\sim$ 10%). We also extended the data coverage of the 3–5 μm stretching region where the ν_3 (2079 cm^{-1}), ν_2 (2274 cm^{-1}), and ν_1 (3327 cm^{-1}) fundamentals are located. Our extended listing spans the 2030–3360 cm^{-1} wavenumber interval and features rest-frequencies with a precision better than 5×10^{-4} cm^{-1} for all lines, including the ones of the ν_1 and $\nu_1 + \nu_7 - \nu_7$ bands which showed evidence of local perturbations in the previous data release [6]. Furthermore, the list of predicted rest-frequencies for the new $\nu_2+2\nu_7-2\nu_7$, and $\nu_3 + 2\nu_7 - 2\nu_7$ hot bands stand as a new addition from the present analysis effort. To summarize, we included in HITRAN rovibrational transitions belonging to the ten bands marked with an asterisk in Table 1.

As far as diacetylene is concerned, HITRAN editions up to 2020 lack information about the ν_4 band. Indeed, previously this band was studied only in a preliminary manner and limited to low-J levels [9,13,25] as the analyses are difficult due to the presence of various accidental resonances. An extended line list spanning the 3297–3365 cm^{-1} range has been computed for rotational levels up to $J = 115$ with an accuracy better than 0.001 cm^{-1}. The line strengths have been calculated following the guideline described above and using the ν_4 absolute intensities measurements of Jolly et al. [36] as a main source of information.

6. Conclusions

In this paper we present a significant improvement in the knowledge of ro-vibrational spectra of HC_3N and HC_4H, two critical species for astrochemistry and planetology. For HC_3N, we significantly extended our previous global analysis [6] by including vibrational levels up to an energy of 1300 cm^{-1}. They include the $\upsilon_5 = 2$ bending overtone and other four vibrational excited states involved in the resonance polyad. The accurate energy positions of these ro-vibrational levels may serve as guidance to identify cyanoacetylene in hot core environments, where vibrationally excited HC_3N is routinely detected at millimeter regime with present day facilities (e.g., ALMA [37]). More importantly, the rest frequencies of the strong $2\nu_5$ band are now predicted with very high accuracy and the relevant data listing has been incorporated in the HITRAN2024 [23] as a new addition. They are important for future observations with the James Webb Space Telescope (JWST), which can target the 7.5 μm region with its medium-resolution MIRI spectrograph. The characterization of the ν_1, ν_2 and ν_3 stretching bands of HC_3N has also been improved, with the analysis of new hot bands and the detailed treatment of the localized perturbations affecting the ν_1 manifold. These data have been updated in the HITRAN2024 edition.

For diacetylene, we implemented the explicit treatment of the perturbations, that affect the ν_4-band system and the resulting spectral predictions have been collected into a novel HITRAN2024 contribution, having the aim of guiding astronomical observations at 3 μm. It is to be kept in mind that HC_4H is a non-polar species, thus its identification in remote environments rely entirely on the signals of its few IR-active vibrational bands.

In summary, this paper keeps on boosting the already considerable spectroscopic knowledge of HC_3N and HC_4H. Despite the high level of details achieved, perspectives for future investigations are still open. For example, the vibrational energy manifold of HC_3N below 1300 cm^{-1} features the $\upsilon_5 = \upsilon_6 = 1 \sim (\upsilon_6 = 1, \upsilon_7 = 3)$ dyad of interacting levels which has not yet been the subject of an exhaustive study. Another stimulating task is the detailed analysis of the $2\nu_5 + \nu_7 - \nu_7$ hot band that contributes with strong signals to the $2\nu_5$ system band pattern. A major difficulty in pursuing this aim is the increase in size of the relevant resonance system, which would consist of 9 vibrational levels, including the first combination with three bending quanta simultaneously excited ($\nu_5 = \nu_6 = \nu_7 = 1$). Tackling the analysis of the ν_4 hot band system of HC_4H with the aim of improving the spectral coverage of the HITRAN database can be viewed as another interesting but challenging task, due to the presence of numerous local perturbations.

CRediT authorship contribution statement

Luca Bizzocchi: Writing – review & editing, Writing – original draft, Validation, Supervision, Software, Resources, Methodology, Investigation, Formal analysis, Data curation, Conceptualization. **Mattia Melosso:** Writing – review & editing, Writing – original draft, Visualization, Validation, Supervision, Resources, Methodology, Investigation, Formal analysis, Data curation, Conceptualization. **Filippo Tamassia:** Writing – review & editing, Validation, Supervision, Investigation, Data curation, Conceptualization. **Martina Taddia:** Writing – review & editing, Investigation, Formal analysis, Data curation. **Francesca Tonolo:** Writing – review & editing, Validation, Investigation, Data curation. **Silvia Alessandrini:** Writing – review & editing, Validation, Investigation, Data curation. **Gabriele Panizzi:** Writing – review & editing, Validation, Formal analysis, Data curation. **Michela Nonne:** Writing – review & editing, Validation, Investigation, Data curation. **Marie-Aline Martin-Drumel:** Writing – review & editing, Validation, Supervision, Resources, Methodology, Investigation, Data curation, Conceptualization. **Olivier Pirali:** Writing – review & editing, Validation, Supervision, Resources, Methodology, Data curation, Conceptualization. **Luca Dore:** Writing – review & editing, Validation, Supervision, Resources, Methodology, Conceptualization. **Iouli E. Gordon:** Writing – review & editing, Validation, Supervision, Resources, Methodology, Investigation, Data curation, Conceptualization. **Cristina Puzzarini:** Writing – review & editing, Writing – original draft, Validation, Supervision, Resources, Methodology, Investigation, Funding acquisition, Conceptualization.

Declaration of competing interest

The authors declare that they have no known competing financial interests or personal relationships that could have appeared to influence the work reported in this paper.

Acknowledgments

This work has been performed under the SOLEIL proposal #20230352; we acknowledge the SOLEIL facility for provision of synchrotron radiation and would like to thank the AILES beamline staff for their assistance. This work has been supported by MUR (PRIN Grant Numbers 202082CE3T, P2022ZFNBL and 20225228K5) and by the University of Bologna (RFO funds). We acknowledge funding from Scuola Normale Superiore (SNS) for supporting this research activity in the framework of the joint SNS-INSTM-University of Bologna "Astrochemistry – Materials under extreme conditions: clues from the gas phase" project. M.M. thanks the European Union – Next Generation EU under the Italian National Recovery and Resilience Plan (PNRR M4C2, Investment 1.4 – Call for tender n. 3138 dated 16/12/2021-CN00000013 National Centre for HPC, Big Data and Quantum Computing (HPC) – CUP J33C22001170001). The COST Action CA21101 "COSY - Confined molecular systems: from a new generation of materials to the stars" is also acknowledged.

Appendix A. Supplementary data

Supplementary material related to this article can be found online at https://doi.org/10.1016/j.jqsrt.2026.109879.

Data availability

The data are provided as supplementary material.

References

[1] Endres CP, Schlemmer S, Schilke P, Stutzki J, Müller HS. The Cologne Database for Molecular Spectroscopy, CDMS, in the Virtual Atomic and Molecular Data Centre, VAMDC. J Mol Spectrosc 2016;327:95–104. http://dx.doi.org/10.1016/j.jms.2016.03.005.

[2] McGuire BA. 2021 census of interstellar, circumstellar, extragalactic, protoplanetary disk, and exoplanetary molecules. Astrophys J Suppl Ser 2022;259(2):30.

[3] Bizzocchi L, Tamassia F, Laas J, Giuliano BM, Degli Esposti C, Dore L, Melosso M, Canè E, Pietropolli-Charmet A, Müller HSP, Spahn H, Belloche A, Caselli P, Menten KM, Garrod RT. Rotational and high-resolution infrared spectrum of HC_3N: global ro-vibrational analysis and improved line catalog for astrophysical observations. Astrophys. J Suppl S. 2017;233:11(20pp). http://dx.doi.org/10.3847/1538-4365/aa9571.

[4] Kunde V, Aikin A, Hanel R, Jennings D, Maguire W, Samuelson R. C_4H_2, HC_3N and C_2N_2 in Titan's atmosphere. Nature 1981;292(5825):686–8.

[5] Malek SE, Cami J, Bernard-Salas J. The Rich Circumstellar Chemistry of SMP LMC 11. Astrophys J 2012;744:16.

[6] Tamassia F, Bizzocchi L, Melosso M, Martin-Drumel M-A, Pirali O, Pietropolli Charmet A, Canè E, Dore L, Gordon IE, Guillemin J-C, Giuliano BM, Caselli P, Alessandrini S, Barone V, Puzzarini C. Synchrotron-based far-infrared spectroscopy of HC_3N : Extended ro-vibrational analysis and new line list up to 3360 cm^{-1}. J Quant Spectrosc Ra. 2022;279:108044.

[7] Bizzocchi L, Tamassia F, Degli Esposti C, Fusina L, Canè E, Dore L. High-resolution infrared spectroscopy of diacetylene below 1000 cm^{-1}. Mol Phys 2011;109(17–18):2181–90.

[8] Bizzocchi L, Degli Esposti C, Dore L. Submillimetre-wave spectrum of diacetylene and diacetylene-d_2. Mol Phys 2010;108:2315–23.

[9] Guelachvili G, Craig AM, Ramsay DA. High-resolution Fourier studies of diacetylene in the regions of the ν_4 and ν_5 fundamentals. J Mol Spectrosc 1984;105:156.

[10] Arié E, Johns JWC. The bending energy levels of C_4H_2. J Mol Spectrosc 1992;155:195.

[11] McNaughton D, Bruget DN. The high-resolution infrared spectrum of diacetylene and structures of diacetylene, triacetylene and dicyanoacetylene. J Mol Struct 1992;273:11.

[12] Jolly A, Fayt A, Benilan Y, Jacquemart D, Nixon C, Jennings D. The ν_8 bending mode of diacetylene: from laboratory spectroscopy to the detection of ^{13}C isotopologues in Titan's atmosphere. Astrophys J 2010;714(1):852.

[13] Zhao D, Doney KD, Linnartz H. High-resolution infrared spectra of vibrationally excited HC_4H in a supersonic hydrocarbon plasma jet. J Mol Spectrosc 2014;296:1.

[14] Yamada KMT, Moravec A, Niedenhoff M, Bürger H, Winnewisser G. Diode laser spectrum of HCCCN: CN stretching band. Z. Naturforsch. 1996;51:27. http://dx.doi.org/10.1515/zna-1996-1-205.

[15] Jiang N, Melosso M, Tamassia F, Bizzocchi L, Dore L, Canè E, Fedele D, Guillemin J-C, Puzzarini C. High-resolution infrared spectroscopy of DC_3N in the stretching region. Front Astron Space Sci 2021;8:29.

[16] Armitage JB, Jones RH, Whiting MC. Researches on acetylenic compounds. Part XXVIII. new route to diacetylene and its symmetrical derivatives. J Chem Soc 1951;44.

[17] Brubach J-B, Manceron L, Rouzières M, Pirali O, Balcon D, Kwabia-Tchana F, Boudon V, Tudorie M, Huet T, Cuisset A, Roy P. Performance of the AILES THz-Infrared beamline at SOLEIL for high resolution spectroscopy. WIRMS 2009 AIP Conf Proc 2009;1214:81–4. http://dx.doi.org/10.1063/1.3326359.

[18] Pirali O, Boudon V, Oomens J, Vervloet M. Rotationally resolved infrared spectroscopy of adamantane. J. Chem Phys 2012;136:024310. http://dx.doi.org/10.1063/1.3666853.

[19] Pirali O, Goubet M, Huet TR, Georges R, Soulard P, Asselin P, Courbe J, Roy P, Vervloet M. The far infrared spectrum of naphthalene characterized by high resolution synchrotron FTIR spectroscopy and anharmonic DFT calculations. Phys. Chem Chem Phys 2013;15:10141–50. http://dx.doi.org/10.1039/c3cp44305a.

[20] Faye M, Bordessoule M, Kanouté B, Brubach J-B, Roy P, Manceron L. Improved mid infrared detector for high spectral or spatial resolution and synchrotron radiation use. Rev Sci Instrum 2016;87:063119. http://dx.doi.org/10.1063/1.4954405.

[21] Melosso M, Degli Esposti C, Dore L. Terahertz Spectroscopy and Global Analysis of the Rotational Spectrum of Doubly Deuterated Amidogen Radical ND_2. ApJS 2017;233(15).

[22] Claus JA, Melosso M, Maillard AA, Bizzocchi L, Barone V, Puzzarini C. Deciphering the complexity in the rotational spectrum of deuterated ethylene glycol. ACS Earth Space Chem 2025;9(5):1267–76.

[23] Gordon IE, Rothman LS, Hargreaves RJ, Gomez FM, Bertin T, Hill C, Kochanov RV, Tan Y, Wcisło P, Makhnev VY, Bernath PF, Birk M, Boudon V, Campargue A, Coustenis A, Drouin BJ, Gamache RR, Hodges JT, Jacquemart D, Mlawer EJ, Nikitin AV, Perevalov VI, Rotger M, Robert S, Tennyson J, Toon GC, Tran H, Tyuterev VG, Adkins EM, Barbe A, Bailey DM, Bielska K, Bizzocchi L, Blake TA, Bowesman CA, Cacciani P, Čermák P, Császár AG, Denis L, Egbert SC, Egorov O, Ermilov AY, Fleisher AJ, Fleurbaey H, Foltynowicz A, Furtenbacher T, Germann M, Guest ER, Harrison JJ, Hartmann J-M, Hjältén A, Hu S-M, Huang X, Johnson TJ, Jóźwiak H, Kassi S, Khan MV, Kwabia-Tchana F, Lee TJ, Lisak D, Liu A-W, Lyulin OM, Malarich NA, Manceron L, Marinina AA, Massie ST, Mascio J, Medvedev ES, Meshkov VV, Mellau GC, Melosso M, Mikhailenko SN, Mondelain D, Müller HSP, O'Donnell M, Owens A, Perrin A, Polyansky OL, Raston PL, Reed ZD, Rey M, Richard C, Rieker GB, Röske C, Sharpe SW, Starikova E, Stolarczyk N, Stolyarov AV, Sung K, Tamassia F, Terragni J, Ushakov VG, Vasilchenko S, Vispoel B, Vodopyanov KL, Wagner G, Wójtewicz S, Yurchenko SN, Zobov NF. The HITRAN2024 molecular spectroscopic database. J Quant Spectrosc Rad. Trans 2026;353:109807. http://dx.doi.org/10.1016/j.jqsrt.2026.109807.

[24] Buijs HL, Ramsay DA. The ν_4 band of diacetylene near 3 microns. Astrophys J Lett 1980;235:L115–7. http://dx.doi.org/10.1086/183170.

[25] Chang C-H, Nesbitt DJ. Spectroscopy and dynamics of jet-cooled polyynes in a slit supersonic discharge: Sub-Doppler infrared studies of diacetylene HCCCH. J Phys Chem A 2015;119(28):7940–50. http://dx.doi.org/10.1021/acs.jpca.5b02310, PMID: 25919691.

[26] Yamada KMT, Birss FW, Aliev MR. Effective Hamiltonian for polyatomic linear molecules. J. Mol Spectrosc 1985;112:347.

[27] Brown JM, Hougen JT, Huber K-P, Johns JWC, Kopp I, Lefebvre-Brion H, Merer AJ, Ramsay DA, Rostas J, Zare RN. The labeling of parity doublet levels in linear molecules. J. Mol Spectrosc 1975;55:500.

[28] Hougen J-T. Rotational Energy Levels of a Linear Triatomic Molecule in a $^2\Pi$ Electronic State. J Chem Phys 1962;36:519.

[29] Watson JKG. The vibration-rotation hamiltonian of linear molecules. Mol Phys 1970;19:465.

[30] DeLeon RL, Muenter JS. Molecular beam electric resonance study of the ground and excited states of cyanoacetylene. J. Chem Phys 1985;82:1702–4. http://dx.doi.org/10.1063/1.448402.

[31] Thorwirth S, Müller HSP, Winnewisser G. The Millimeter- and Submillimeter-Wave Spectrum of HC_3N in the Ground and Vibrationally Excited States. J Molec. Spectrosc 2000;204:133.

[32] Pickett HM. The fitting and prediction of vibration-rotation spectra with spin interactions. J Mol Spectrosc 1991;148(2):371–7.

[33] Aliev MR, Watson JKG. In: Rao KN, editor. In: molecular spectroscopy: modern research, vol. III, New York: Academic Press; 1985, p. 1–67.

[34] Gordon IE, Rothman LS, Hargreaves RJ, Hashemi R, Karlovets EV, et al. The HITRAN2020 molecular spectroscopic database. J Quant Spectrosc Rad. Trans 2021;107949. http://dx.doi.org/10.1016/j.jqsrt.2021.107949.

[35] Jolly A, Benilan Y, Fayt A. New infrared integrated band intensities for HC_3N and extensive line list for the ν_5 and ν_6 bending modes. J. Mol Spectrosc 2007;242:46–54. http://dx.doi.org/10.1016/j.jms.2007.01.008.

[36] Jolly A, Manceron L, Kwabia-Tchana F, Benilan Y, Gazeau M-C. Revised infrared bending mode intensities for diacetylene (C_4H_2): application to Titan. Planet Space Sci 2014;97:60.

[37] Chen L, Qin S-L, Liu T, Goldsmith PF, Liu X, Peng Y, Tang X, Garay G, Kou Z, Tang M, et al. The ALMA-ATOMS survey: Vibrationally excited HC_3N lines in hot cores. Astron Astrophys 2025;694:A166.